Arabian Journal of Chemistry (2021) **14**, 103242

King Saud University

Arabian Journal of Chemistry

www.ksu.edu.sa
www.sciencedirect.com

ORIGINAL ARTICLE

The making of a high performance supercapacitor active at negative potential using sulphonic acid activated starch-gelatin-TiO_2 nano-hybrids

O.D. Saliu, M. Mamo, P. Ndungu, J. Ramontja *

Department of Chemical Sciences, University of Johannesburg, P.O. Box 17011, Doornfontein 2028 Johannesburg, South Africa

Received 24 January 2021; accepted 30 May 2021
Available online 09 June 2021

KEYWORDS

Starch biopolymers;
Nanogelatin;
Supercapacitor;
Energy storage;
Negative voltage

Abstract This work reports the design of nano-level starch-gelatin biopolymeric blends incorporated with nano-TiO_2 for energy storage applications in areas which need to utilise negative voltages. Six different activated nanoarchitectures were designed, push coated on nickel foam substrates and characterized with FTIR, a Zeta sizer, XRD, TEM, CV, EIS, and GCD techniques for structural, functional and electrochemical properties respectively. The C—O—C glucosidic linkage, amide A bond, Ti—O bond were seen at 1068, 2783, 602 cm^{-1} to confirm the succesful synthesis of starch-gelatin-TiO_2 nanohybrids, while TEM confirmed well dispersed TiO_2 NPs dispersed within the crystalline starch nanoparticles and oval shaped nano-gelatin NPs. XRD analysis revealed crystallite sizes to be in the range of 21–98 nm for all nano-architectures, and confirmed the prescence of highly ordered phases suitable for energy storage, after activation. The zeta sizer investigations determined that the samples were nanoparticulates with sizes below 100 nm. The highest specific capacitances obtained at 5 mVs^{-1} were 237, 246, 349, 686, 691, 808F/g in the three electrodes configuration and 194, 204, 287, 541, 570, 617F/g in the two electrodes configurations for AS-NPs, AG-NPs, ASG-NHs, AS-TiO_2 NHs, AG-TiO_2-NHs and ASG-TiO_2-NHs respectively. When the samples were tested using a three-electrode and two-electrode configuration, the activated starch-gelatin-TiO_2 nanohybrid showed the lowest R_{ct} of 0.28 Ω and 0.51 Ω, energy densities of 208.3 and 176.4 Wh/Kg, and power densities of 6213 and 5406 W/Kg. All samples had retention capacities of 86–95%, with the activated starch-gelatin-TiO_2 nanohybrid having values of 95% and 92% for the GCD experiments run using three and two electrode configurations. This work demonstrates that biopolymer nanohybrids can be effective electrodes for supercapacitors devices in energy storage applications.

* Corresponding author.
E-mail address: jamesr@uj.ac.za (J. Ramontja).
Peer review under responsibility of King Saud University.

Production and hosting by Elsevier

1. Introduction

Negative voltage supplies are needed in op-amp circuits and audio amplifiers (Kim et al., 2014; Liu and Zeng, 2018). Some recent reports, in the open literature, have also shown that

https://doi.org/10.1016/j.arabjc.2021.103242
1878-5352

negative voltages improve the corrosion resistance of coatings on metal plates thus extending the life span of the protective barriers (Liu and Zeng, 2018). Other applications where negative voltages can be advantageous include in signal conditioning, smart switches, sensors and semiconductor memory devices. Modern supercapcitors should be designed and fabricated into such dynamic areas of applications, in order to meet the demands of the fourth industrial revolution (4IR). Energy storage systems are crucial for the development and functionality of novel integrated devices, and must be designed in such a way that addresses the need for high demand portable and sustainable energy devices (Liu and Zeng, 2018; Wang et al., 2014). To meet the demand within the evolving and growing nexus of the fourth industrial revolution, the application of biopolymer based supercapcitors into areas of signal and switch controls, portable and/or wearable energy storage and supply, may bridge the gap between power physics and energy chemistry (J. Li et al., 2019). Supercapacitors offer a means to deliver and store energy on demand in a well controlled fashion, and their economic benefits allow for easier commercialization and distribution (Gopi et al., 2020), especially in the context of a developing economy.

The configuration and physicochemical characteristics of the material of an electrode are some of the most important factors that need to be considered when designing supercapacitors for electronic devices and hybrid vehicles (Pant et al., 2019). The material, and its nanostructural architecture, determines the ion diffusion, charge–discharge characteristics and the overall chemistry of the surfaces of soft and hard electrochemical matrices. Hence, there is a need to fabricate more diversified and sustainable electrodes if unique electrochemical performances are desired in the world of energy materials (Wang et al., 2015). As a result, there are continual drives and novel developments that seek to manipulate and tailor the conductivity and morphology of biopolymeric electrode templates for energy storage applications. Recently, sustainable, clean and greener electrodes are gaininng wider attention for applications in the areas of energy storage. Several recent reports have shown that polysaccharides and other related biomaterials can be employed as electrodes and not only as binders and electrolytes in supercapcitor applications (Kasturi et al., 2019; Selvaraj et al., 2020)

Conductivity of biopolymers can be improved by activating them, or doping, with nanomaterials, introduction of certain functional groups, co-polymers, or special conductive liquids which induces polarons, bipolarons and electronic radicals that travel throughout the polymeric chains by various mechanisms, including diffusion (Finkenstadt, 2005; Ibanez et al., 2018). Another way to enhance the electrochemical properties of biopolymeric capacitive electrodes is to employ activated or doped polysaccarides with good chemical stability sandwiched with pseudo-capacitive nano-transition metal oxides (nTMO) (Chong et al., 2019; Yan et al., 2017). These nTMOs contribute to faster electron kinetics, high power density, exceptional life cycle, wide operating temperature range. One nTMO of particular interest is TiO_2, due to the abundance of its ores within South Africa (Rozendaal et al., 2018), national beneficiation strategies (Oosthuizen and Swanepoel, 2018), and when combined with nano-carbons or polymers, it offers superb electrochemical activity and exceptionally high specific energy density (Liu et al., 2009; Elmouwahidi et al., 2018; Kumar et al., 2020; Khan et al., 2019).

Pant et al., reported on the synthesis of TiO_2-carbon nanofibre for supercapcitor applications and obtained specific capacitance (C_{sp}) of 107 Fg^{-1} at a current density of 1 Ag^{-1} with a capacity retention of 84% at 2000th cycle. Lal et al., also fabricated a composite of copper, copper oxide and carbon nano-fiber incorporated with TiO_2 and obtained a high C_{sp} value of 530F/g at 1.5 Ag^{-1} current density with 45.83 Wh/Kg and 1.27 kW/Kg respective energy and power density. From other research on supercapacitor electrolytes, gelatin biopolymers have been confirmed to posses short ionic diffusion path length and therefore were used for solid electrolytes with high bending resistance. (Lal et al., 2019; Pant et al., 2019; Railanmaa et al., 2019). Fan et al., further designed gelatin based microporous sheets with a 76% capacity retention at a C_{sp} of 20 A/g. Thus, we anticipate that gelatin may impart good electron transfer kinetics and bending resistance properties to a starch nano-matrix composite, when hybridized in a suitable manner.

The nano-starch biopolymer will hence be a compatible agent because of similar bond structure it has with gelatin and it will also help to optimize its low retention capacity. The TiO_2 used also has proved to alleviate volumetric variations and does not support dendrite growths, thereby reducing any form of nucleation overpotential during charging (Zhou et al., 2019). In addition, polysaccharides based nanoarchiteronics provides extensibility, flexibility and fast doping-dedoping cycle (Fan and Shen, 2015; Pant et al., 2019). The research subject of this work is centred on the use of starch and gelatin nanoarchitectures. The novelty of this work resides in the use of nano level gelatin and starch for the design of supercapacitor electrodes having optimal electrochemical performance at negative voltages for potential applications in signal control systems and smart switches, and devices for future 4IR applications. It provides a platform for the design of symmetrical supercapacitors which can easily switch polarities in areas which requires both positive and negative voltages. This new nano-form of gelatin and starch biopolymers offers tunable transport properties and unique surface chemistry more than their conventional bulk counterparts. The incorporated TiO_2 further works as a template for pore creation.

Table 1 Conductivity of starch and gelatin, before and after activation, with respect to temperature in °C.

Conductivity (μScm^{-1})	Temperature (°C)							
	30	40	50	60	70	80	90	100
Starch	4.47	4.49	4.93	4.98	5.05	5.42	6.10	6.02
Activated starch	16.31	18.72	22.94	22.66	26.81	26.45	27.90	30.05
Gelatin	4.61	4.81	5.15	5.42	4.93	5.85	6.37	6.31
Activated gelatin	18.09	22.5	31.77	44.23	49.09	59.88	67.15	68.17

The activation process converts both starch and gelatin biopolymers into more ordered and conductive phases.

2. Methodology

All reagents were purchased from Sigma Aldrich, South Africa. All glassware and other vessels used, were washed with deionized water and air dried before use.

2.1. Design of activated starch and gelatin nanoparticles

The hydrolysis method, which involves sulfuric acid, was adapted and modified from literature (Ding et al., 2010; Tay et al., 2012). A mixture of 30 g starch, 1.5 g of *para*-toluene sulphonic acid (PTSA) and 500 mL of 3.1 M H_2SO_4, was stirred for 2 h at 100 rpm (stirring speed) at 40 °C. The mixture was then placed in a microwave oven, and subjected to a microwave treatment protocol that consisted of a 30-second exposure to 100 W of microwave energy, and then a rest cycle for 1 min. This was repeated several times over a period of an hour, until the mixture changed from white to a brown colour. The suspension produced was mixed with 15% methanol without stirring and successively centrifuged and stored under a fume hood until the gelatine was ready for the next step (Ding et al., 2010; Tay et al., 2012). The polyol emulsion method was adopted and modified (Houshyari et al., 2018). A mixture of 10 g of gelatine and 200 mL of mixed polyols (50% tergitols and 50% of styrol solution) was heated to a temperature of 60 °C for 1 h using a hot plate. The suspension was treated with 20 mL of 0.1 M HCl and 1.0 g of *para*-toluene sulphonic acid and left standing, without any agitation, under a fume hood for a period of 2 hours The mixture was then centrifuged and the gelatine material stored under ambient conditions.

2.2. Fabrication of nanoarchitectures of starch, gelatin and TiO_2

Distilled water, 200 mL, was mixed with 1 g of urea in a double-necked round bottom flask and the resultant mixture was heated at 75 °C and allowed to reflux for fifteen minutes. Then, 50 mL of Titanium isopropoxide was added drop-wise, over a period of 5 min, and the suspension produced was then stirred for one hour at 90 °C, in a water bath. The obtained powder was then separated (centrifuge, 2500 gcf) and dried at 80 °C in an oven. The synthesis of TiO_2 was adapted from the literature (Dodoo-Arhin et al., 2018; REDDY et al., 2001). Activated starch nanoparticles (AS-NPs), activated gelatin nanoparticles (AG-NPs), activated starch-gelatin nanohybrids (ASG-NH), activated starch-TiO_2 (AS-TiO_2 NH), activated gelatin-TiO_2 (AG-TiO_2 NH), and activated starch-gelatin-TiO_2 (ASG-TiO_2 NH) were designed by stabilization of respective nano-biopolymers in 20 mL of 50:50 tween-80 and isobutanol solution under stirring for 2 h. To obtain the nanocomposite powders, the mixtures were dried at 50 °C in an oven (~8 hours), and then kept in a desiccator until characterization.

2.3. Material characterizations

Attenuated Total Reflection-Fourier Transform Infra-Red (ATR-FTIR) was performed on a Spectrum-100 Perkin Elmer (USA) instrument, from 4000 to 600 cm^{-1} wavenumbers. The X-ray diffraction (XRD) measurements were done using a Rigaku Ultima IV, X-ray diffractometer (Japan) using Cu-Kα radiation of 1.5406 Å generated at 45 kV and 40 mA. The diffraction patterns were obtained over a 2-theta values ranging from 5° to 90°, using a step size of 0.01° and 1°/min scan rate. A TESCAN VEGA (Czech Republic) scanning electron microscope (SEM) was employed to study the surface morphology of the samples, using a 20 kV accelerating voltage. The particle sizes of the nano-hybrids were investigated using a Dynamic Light Scattering (DLS) instrument, Zetasizer, model: ZEN 3600.

2.4. Electrochemical studies

The principle of push loading was employed to coat 20 mg of homogenous pastes, of the prepared biopolymeric nanoarchitectures, on dried nickel foams to form working electrodes. Pastes were prepared by mixing the samples (160 mg) with polyvinylidene fluoride (PVDF) in *N*-methyl-2-pyrrolidone (NMP) (20 mg PVDF: 1.0 g NMP). The electrochemical properties of the nanocomposites were initially investigated using a three-electrode configuration, with a 1 M Na_2SO_4 aqueous electrolyte (at room temperature), a Ag/AgCl reference electrode, and a platinum wire coil as the counter electrode. Cyclic voltammetry measurements, electrochemical impedance spectroscopy (EIS) and galvanostatic charge–discharge (GCD) experiments were performed using a Gamry 1010 E potentiostat. In the two-electrode configuration, the electrodes were prepared as per the method used for the working electrodes in the three-electrode configuration. A glass fibre separator was soaked in 1 M Na_2SO_4 electrolyte and sandwiched in between two symmetrical working electrodes. The symmetrical supercapacitor was aligned and pressed before setting it up for electrochemical measurements.

3. Results and discussion

3.1. Effect of activation of starch and gelatin biopolymers

The starch and gelatin nanoparticles were first activated in the presence of *para*-toluene sulphonic acid and ammonium chloride, then tested for energy storage applications. As reported in previous works (Romero et al., 2013), the activation step leads to p-type doping which creates structural distortions and re-alignment of the polymer chains, and this results in the generation of radical cations (polarons) and double radicals (bipolarons). The activation was confirmed through conductivity studies carried out using the four-probe method, where a four-fold conductivity increase was obtained after activation. At a temperature of 100 °C, the conductivity of starch moved from 6.02 to 30.05 μScm^{-1} after activation, while that of gelatin moved from 6.31 to 68.17 μScm^{-1}. Hence, the activation led to an overall increase in conductivity of the biopolymers (see Table 1).

At 30 °C, the effect of activation resulted in a conductivity of 16. 31 μScm^{-1} in starch, and 18.09 μScm^{-1} in gelatin, indicating that they will not lose their conductance at room temperature, for energy applications. The activation blocks the swelling points of starch and gelatin through ring attachments and creates faster electronic transport channels. This will

enable the starch and gelatin biopolymers to undergo numerous, and possibly higher, charge and discharge cycles. This can be observed in the conductivity values of the un-activated starch and gelatin at temperatures of 90 and 100 °C, where a decrease from 6.10 and 6.37 to 6.02 and 6.31 were observed. This is because the un-activated (ordinary) starch and gelatin biopolymers are now being distorted at high temperatures, hence, they start losing their conductance. After activation, both starch and gelatin retained their high conductivity behaviours, because all swelling points have been blocked.

As depicted in the FTIR spectra presented in Fig. 1a of the starch and gelatin before and after activation, the non-activated starch displayed the expected bands for C—H stretching (between 2750 and 3000 cm^{-1}), C—O stretching, C—H symmetric bending, CH_2 twisting (1250–1500 cm^{-1}), and C—C stretching (500–750 cm^{-1}). After activation, a strong peak was observed at 1708 cm^{-1} to confirm the oxidative products of the starch carbons. Sulphone peaks were also noted at 1311 cm^{-1} and there was a general shift in the C—H vibrational energies of the starch biopolymer into the lower wavelength regions. Similar results were reported in the literature (Fan et al., 2012; Warren et al., 2016). Similar observations were seen with the activated gelatin at the fingerprint region, there are new peaks due to the *para*-aromatic dopant.

The XRD results are presented in Fig. 2a and b. Two prominent peaks were observed with the starch, before activation, at 19.4° and 22.8° 2θ, and the gelatin before activation had wide characteristic peaks at 23.1°, 38.3°, 48.4° and 53.7° 2θ. After activation, the type-A starch was converted into type-B starch. Type-B starches are more crystalline and ordered, as seen with the additional peaks (Fig. 2a), and the characteristic peaks of the type-B starch were noted at 22.8°, 33.3°, and 35.4° 2θ. In addition, after activation, the gelatin also switched from type-B gelatin (or alkaline derived gelatin) into type-A gelatin, which is an acid derived gelatin. The type-A gelatin possess higher degree of crystallinity, as seen with the increased number of peaks. The XRD confirms a phase transition in both the starch and gelatin after activation.

3.2. The design of activated starch and gelatin nano-hybrids

Fig. 3 shows the FTIR spectra of all six fabricated nano-hybrids, and biopolymer-based, electrode materials. Activated starch and activated gelatin were first converted to nano-forms, to make activated starch nanoparticles and activated gelatin nanoparticles. These hybrids were fabricated to form activated starch-gelatin nanohybrids, and three of them were incorporated with TiO_2. For the activated starch nanoparticles, the transmittance peaks at 3408 and 2914 cm^{-1} represents the O—H and C—H stretch vibrations, while the bending vibrations of the methylene groups are shown at 1431 and 1460 cm^{-1} respectively for in and out-of-plane bends (see Fig. 3). The C—O—C linkages of the glycosidic rings are confirmed from the 1068 cm^{-1} peak (Hoyos-Leyva et al., 2017; Sondari et al., 2018).

The successful restructuring of the gelatin, to form nanoparticles, was confirmed using FTIR. The vibrations of amide A, amide I and amide II were seen at 2783 cm^{-1}, 1635 cm^{-1} and 1522 cm^{-1} respectively, and these peak positions are similar to other literature reports (Subara et al., 2018). The activated starch-gelatin nanohybrids showed no change in the amide I peak environment indicating no major change in the secondary structure of activated gelatin nanoparticles after blending with the activated starch nanoparticles. This is in agreement with the report of Chen et al., and Sharma et al., but Kumar et al., further reported the formation of aldimine as a result of the interactions between the carbonyl and the amine groups of the gelatin biopolymers. The C—H overtones between 1400 and 800 cm^{-1} confirmed the mixed helices of both biopolymers without a change in their transmittances as shown from FTIR results (Chen et al., 2017; Kumar et al., 2019; Sharma et al., 2018).

After the incorporation of TiO_2 nanoparticles, the O—H and methylene groups displayed reduced intensities and transmittances, which confirms intermolecular interactions between the Ti—O, C—O and O—H bonds of the starch and gelatin nano-hybrids. Some of the amide bands of the gelatin disappeared, but the glycosidic linkages remained intact and showed

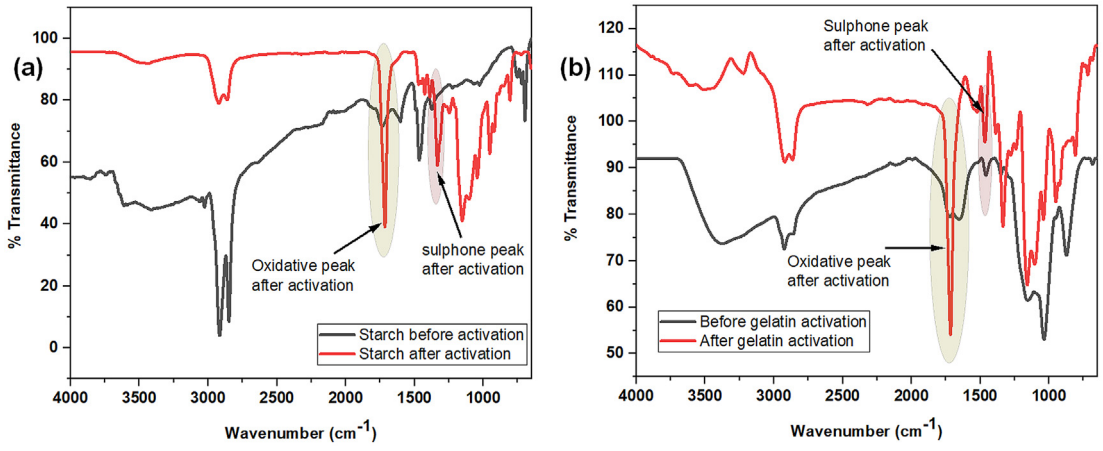

Fig. 1 (a) FTIR of starch, before and after activation (b) FTIR of gelatin, before and after activation.

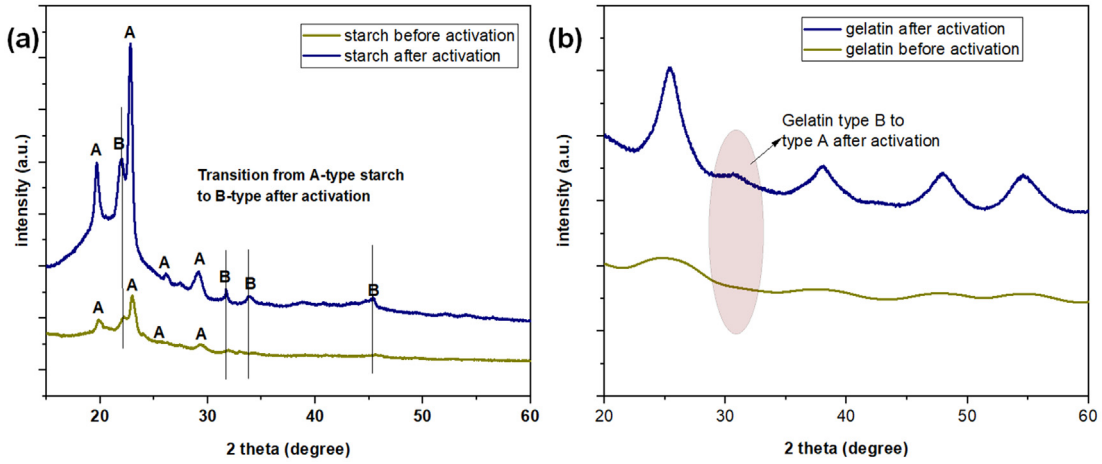

Fig. 2 (a) XRD of starch, before and after activation (b) XRD of gelatin, before and after activation.

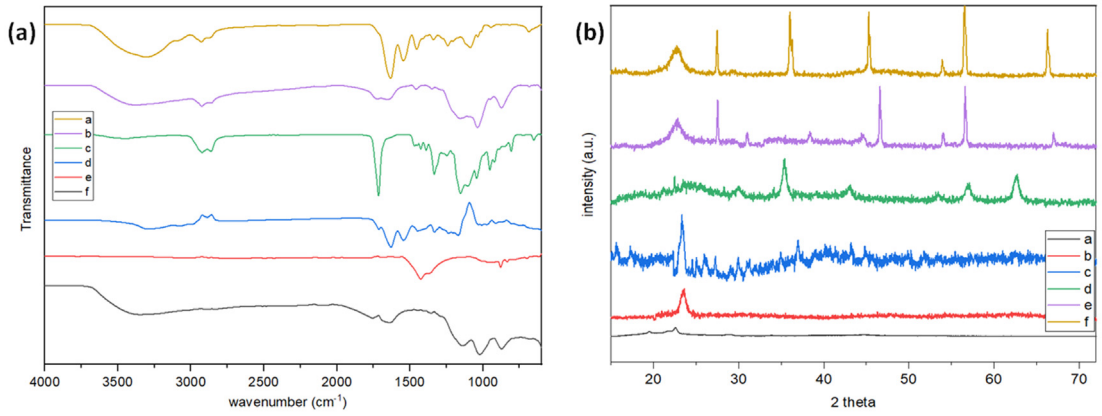

Fig. 3 (I) FTIR and (II) XRD of the activated forms of (a) starch nanoparticles (b) gelatin nanoparticles (c) starch-gelatin naohybrids (d) starch-TiO_2 nanohybrids (e) gelatin-TiO_2 nanohybrids (f) starch-gelatin-TiO_2 nanohybrids.

a shift towards the left at 907 cm^{-1}. The shift is an indication of tight bonding interactions within and between the prepared nano-architectures. The C—O—Ti bond was seen at 1054 cm^{-1} confirming stable Ti—O functionalities after incorporation of TiO_2. Oleyaei et al., (Oleyaei et al., 2016) reported that electrostatic interactions between Ti^{2+} and —OH groups of starch caused wider and flattened bands at 450–800 cm^{-1} while O—H and C—H stretching vibrations moved to longer wavenumbers, similar observations were noted with the nano-architectures prepared in this work. The electromeric effect and hydrogen bonding between the amide groups of gelatin and Ti^{2+} further caused the reduced transmittance and intensity observed in the FTIR spectra of the hybrid nano-architectures, similar results were reported by W. Li et al. (2019).

Histograms displaying the size distributions for the prepared nano-architectural samples are presented in Fig. 4. The activated starch nanoparticles showed an average size of 13 nm, the activated gelatin nanoparticles showed an average size of 79 nm, and the hybrids formed (activated starch-gelatin nanohybrid) had an average particle size of 66 nm. After incorporating TiO_2, the starch-TiO_2 nanohybrid showed an average particle size of 74 nm, the gelatin-TiO_2 nanohybrids had an average size of 93 nm, and the activated starch-gelatin-TiO_2 nanohybrid showed average sizes of 87 nm. The size distributions revealed the nano-hybrids have good dispersibility and low aggregation, favouring a fast electron transfer and kinetics behaviour during impedance studies.

The statistics of the particle sizes indicated a normal distribution, this was similar to the study by Liu et al., 2009. From Gu et al., normal size distributions confirms good capacitive behaviour of the activated polymer matrixes (Gu et al., 2019). In addition, previous works have shown that uniform coating of electrodes can be achieved when the polymers exist at nano-size dimensions; retention capacity decreases quickly when particle sizes are too large. In addition, interfacial impedance of nano-sized electrodes, which have incorporated transition metal oxides and hydroxides are very low during electrode dependant applications (Capone et al., 2019; Hu and Lei, 2007; Wu et al., 2018).

The XRD of the activated starch nanoparticles (Fig. 3II) showed characteristic diffraction peaks at 19.4° and 22.7° as a singlet and doublet respectively to represent the [1 1 1] and [2 2 0] crystal planes (JCPDS 64-1453). The gelatin nanoparticles showed predominant peaks at 26.1°, 38.3° and 49.5° for [1 1 1], [2 0 0] and [2 2 0] respective crystal planes (Marvizadeh

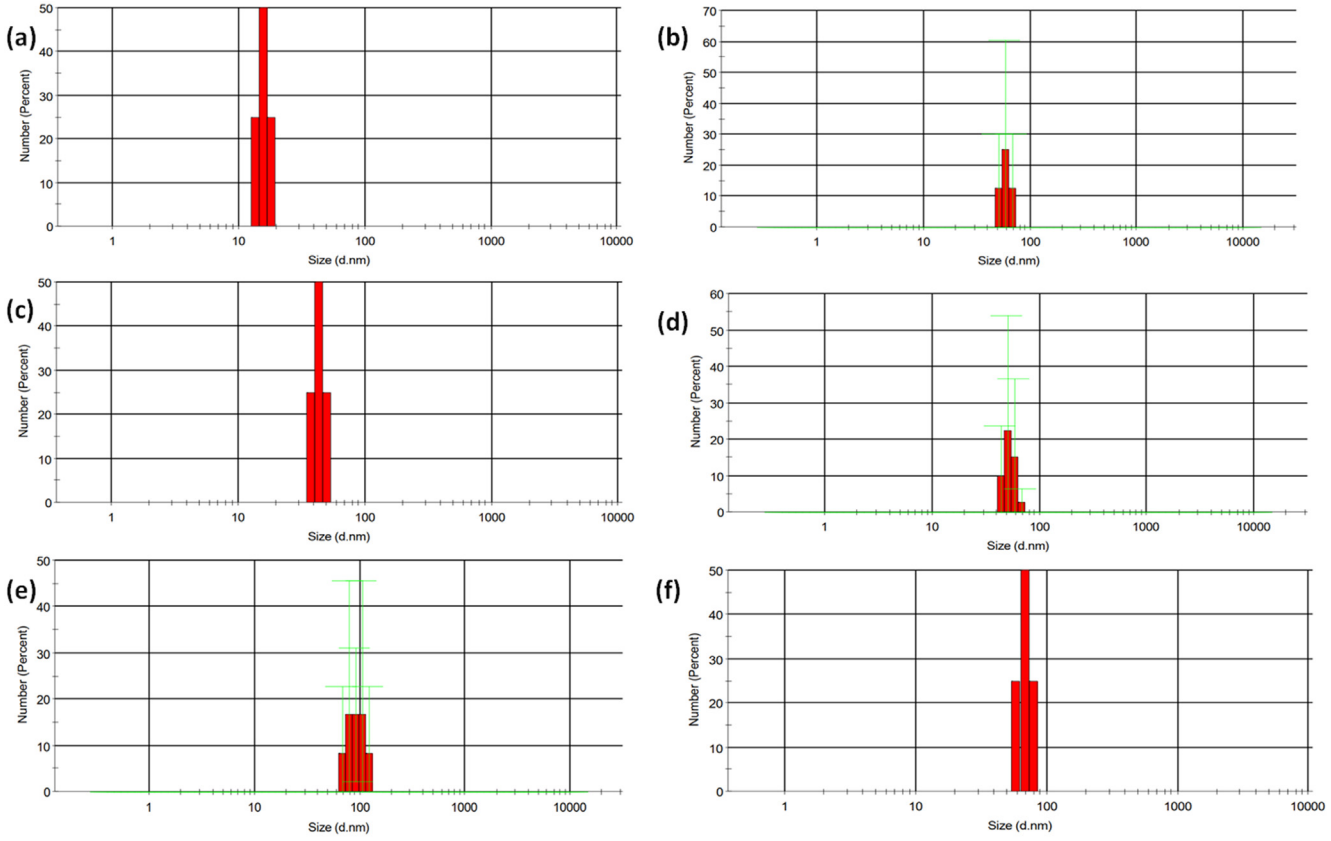

Fig. 4 Particle size histogram of the activated forms of (a) starch nanoparticles (b) gelatin nanoparticles (c) starch-gelatin nanohybrids (d) starch-TiO_2 nanohybrids (e) gelatin-TiO_2 nanohybrids (f) starch-gelatin-TiO_2 nanohybrids.

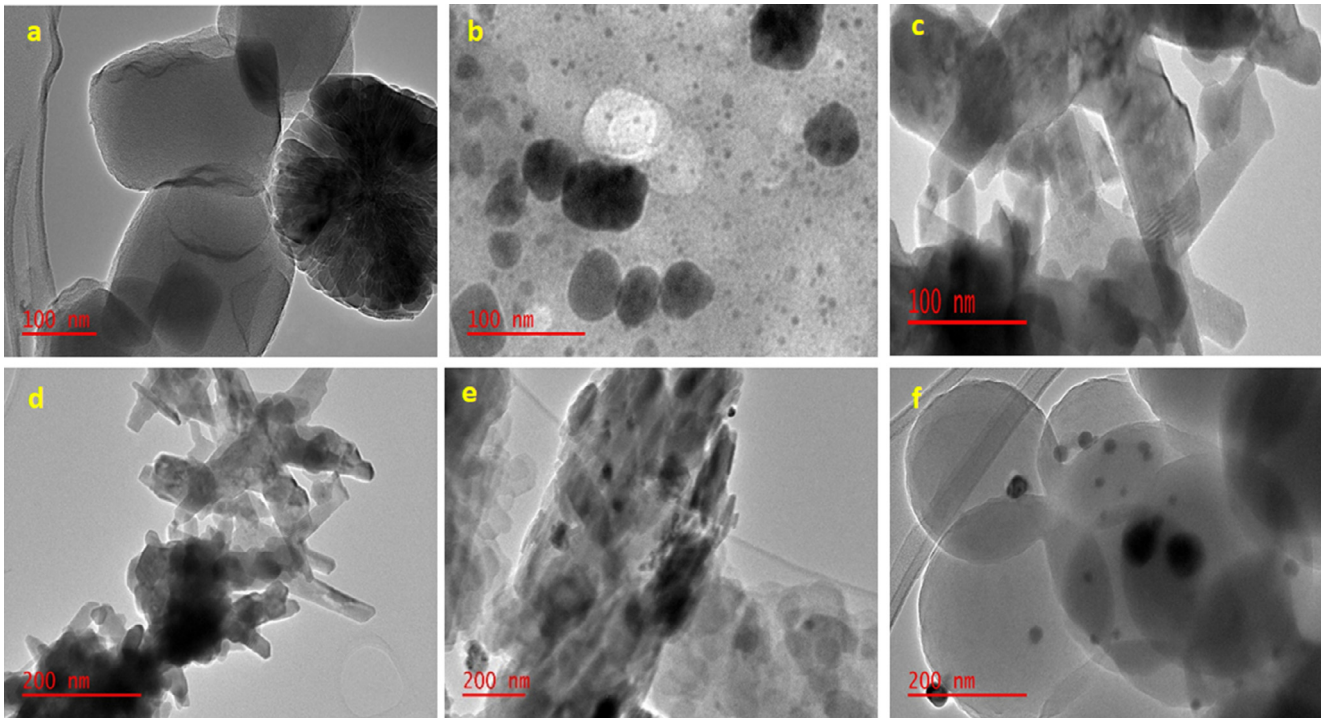

Fig. 5 TEM of the activated forms of (a) starch nanoparticles (b) gelatin nanoparticles (c) starch-gelatin nanohybrids (d) starch-TiO_2 nanohybrids (e) gelatin-TiO_2 nanohybrids (f) starch-gelatin-TiO_2 nanohybrids.

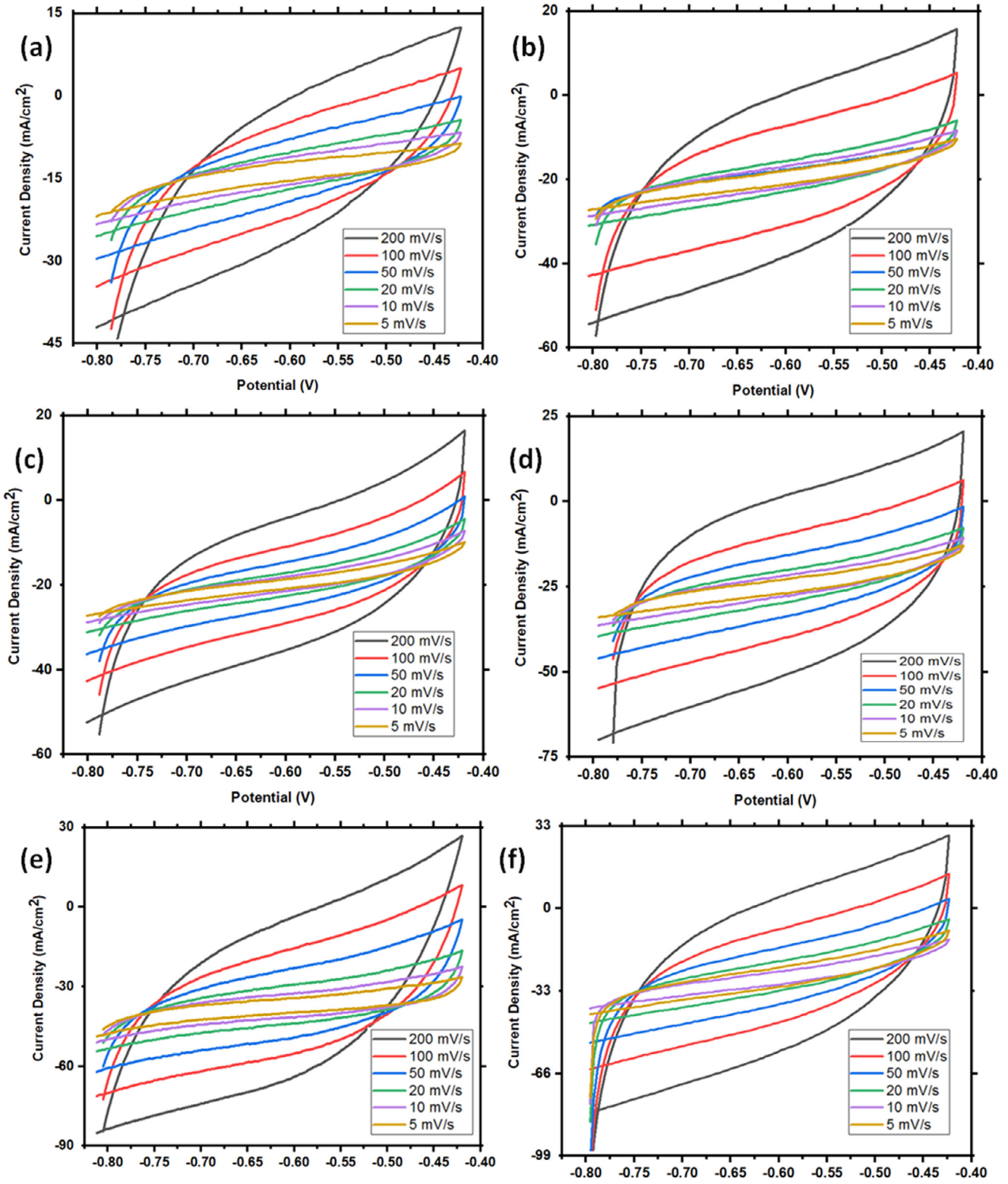

Fig. 6 (Three electrode configuration) CV of the activated forms of (a) starch nanoparticles (b) gelatin nanoparticles (c) starch-gelatin nanohybrids (d) starch-TiO_2 nanohybrids (e) gelatin-TiO_2 nanohybrids (f) starch-gelatin-TiO_2 nanohybrids, at scan rates of 5, 10, 20, 50, 100 and 200 mVs^{-1}.

et al., 2017; Xia et al., 2015). The diffraction peaks at 26.3°, 35.7° and 46.1° confirms the incorporation of titanium dioxide nanoparticles for [1 0 1], [0 0 4] and [2 0 0] crystal planes (JCPDS card no. 78-2486) (Soliman and Furuta, 2014).

The percentage crystallinity of the starch nanoparticle helix remained constant after the blending of both starch and gelatin biopolymers together. A crystallinity of 74 and 71.8% for starch was obtained from the XRD peaks before and after

blending. Although, the intensity of the characteristic crystalline peak of the starch helices remained fairly constant, the intensity of the triple helical structure in the crystalline gelatin at 26.1° decreased progressively with blending (Mendes et al., 2016). The XRD patterns for the TiO_2 incorporated into the various nano-architectures (Fig. 3(II), patterns d, e, and f) appeared to be very similar, and this is due to the strong effect of the TiO_2 crystallinity over the biopolymers.

The TEM analysis was used to establish the successful design of the nano-structured starch and gelatin based architectures. Fig. 5a shows the activated starch nanoparticles with well arranged lamellar and no traces of internal aggregations. The activated gelatin nanoparticles were seen to be oval nanocrystals, and similar to other observation reported in the literature (Jeong and Park, 2014). The absence of aggregation in both activated starch and gelatin nanoparticles corresponds with the particle size distribution results obtained in Fig. 4. In the activated starch-gelatin nanohybrids, the gelatin were seen to be encapsulated within the starch lamellar (Kašlík et al., 2018; Yang et al., 2013). After TiO_2 incorporation, The TiO_2 nanoparticles stayed in well-spaced localized regions within the lattices of the activated starch and gelatin nanoparticles. This good dispersion of the TiO_2 nanoparticles is required for better transfer and storage of charges within supercapacitors (Liu et al., 2009, 2017).

3.3. Three electrode configuration electrochemical study

The electrochemical properties of the nano-hybrids prepared were evaluated using a three electrodes configuration. Cyclic voltammetry (CV), galvanostatic charge–discharge (GCD) experiments, and electrochemical impedance spectroscopy (EIS) were done in a 1 M Na_2SO_4 electrolyte solution. As seen in Fig. 6, the CV curve shows quasi rectangular shapes from 5 to 200 mV/s, indicative of supercapacitive behaviour of the nano-hybrids (Xu et al., 2019). This also shows that the fabricated nano-starch-gel-TiO_2 is free of structural and conformational defects (Xu et al., 2019).

In general, any redox peaks that may be observed with polymer based nanohybrids are due to the presence of polarons and free electrons created after activation (Wang et al., 2015). The CV curves of the electrodes were recorded in the potential range of −0.8 to −0.4 V at scan rates of 5, 10, 20, 50, 100 and 200 mV/s. Surface faradaic reactions, which are responsible for the good performance of the electrodes, include interactions between TiO_2, H^+, and polarons to form TiOOH complex, interaction between TiO_2, N—H and O—H from starch and gelatin to form charge storage domains in excited states (Nagamuthu et al., 2013).

Specific capacitance values were obtained using the area of the CV curves, scan rates and potential windows. Activated starch nanoparticles had specific capacitances (C_{sp}) values of 41, 89, 128, 174, 206 and 237 Fg^{-1} at scan rates of 200, 100, 50, 20, 10 and 5 mVs^{-1} respectively. Activated gelatin nanoparticles had C_{sp} of 77, 96, 125, 169, 212 and 246 Fg^{-1}. Activated starch-gelatin nanohybrids had higher specific capacitance values than those of activated starch and gelatin nanoparticles respectively, showing C_{sp} values of 129, 146, 228, 273, 301 and 349 Fg^{-1}. Values are summarised in Table 2.

After TiO_2 incorporation, activated starch-TiO_2 nanohybrid showed C_{sp} values (Table 2) of 380, 487, 517, 549, 609 and 686 Fg^{-1}. The effect of TiO_2 incorporation led to a greater than five-times increase in the specific capacitance values, with the activated starch. Activated gelatin-TiO_2 nanohybrid showed C_{sp} values of 397, 461, 522, 593, 641 and 691 Fg^{-1}, while activated starch-gelatin-TiO_2 nanohybrids showed C_{sp}

Table 2 Specific capacitance, energy density and constant phase element (CPE) model parameters for the respective nanohybrids prepared, in three electrode configurations.

Sample	Scan rate (mVs^{-1})					
	200	100	50	20	10	5
AS-NPs	41	89	128	174	206	237
AG-NPs	77	96	125	169	212	246
ASG-NH	129	146	228	273	301	349
AS-TiO_2 NH	380	487	517	549	609	686
AG-TiO_2 NH	397	461	522	593	641	691
ASG-TiO_2 NH	286	502	581	644	726	808
	Energy density ($WhKg^{-1}$)					
AS-NPs	12.3	19.7	22.8	36.1	57.3	80.6
AG-NPs	12.9	24.8	26.143.5	43.5	70.41	108.3
ASG-NH	19.1	26.2	26.8	59.2	93.6	126.5
AS-TiO_2 NH	30.8	38.7	43.2	71.0	103.8	137.2
AG-TiO_2 NH	36.3	42.4	49.0	78.6	109.3	159.4
ASG-TiO_2 NH	52.1	61.9	73.6	92.1	145.7	208.3
	R_s	ESR	R_{ct}	W	CPE	n
AS-NPs	0.15	0.110	0.43	2.76	0.151	0.51
AG-NPs	0.15	0.107	0.40	2.71	0.143	0.58
ASG-NH	0.15	0.104	0.39	2.65	0.142	0.59
AS-TiO_2 NH	0.14	0.101	0.34	2.20	0.118	0.61
AG-TiO_2 NH	0.14	0.101	0.31	2.20	0.114	0.63
ASG-TiO_2 NH	0.12	0.087	0.29	1.97	0.112	0.65

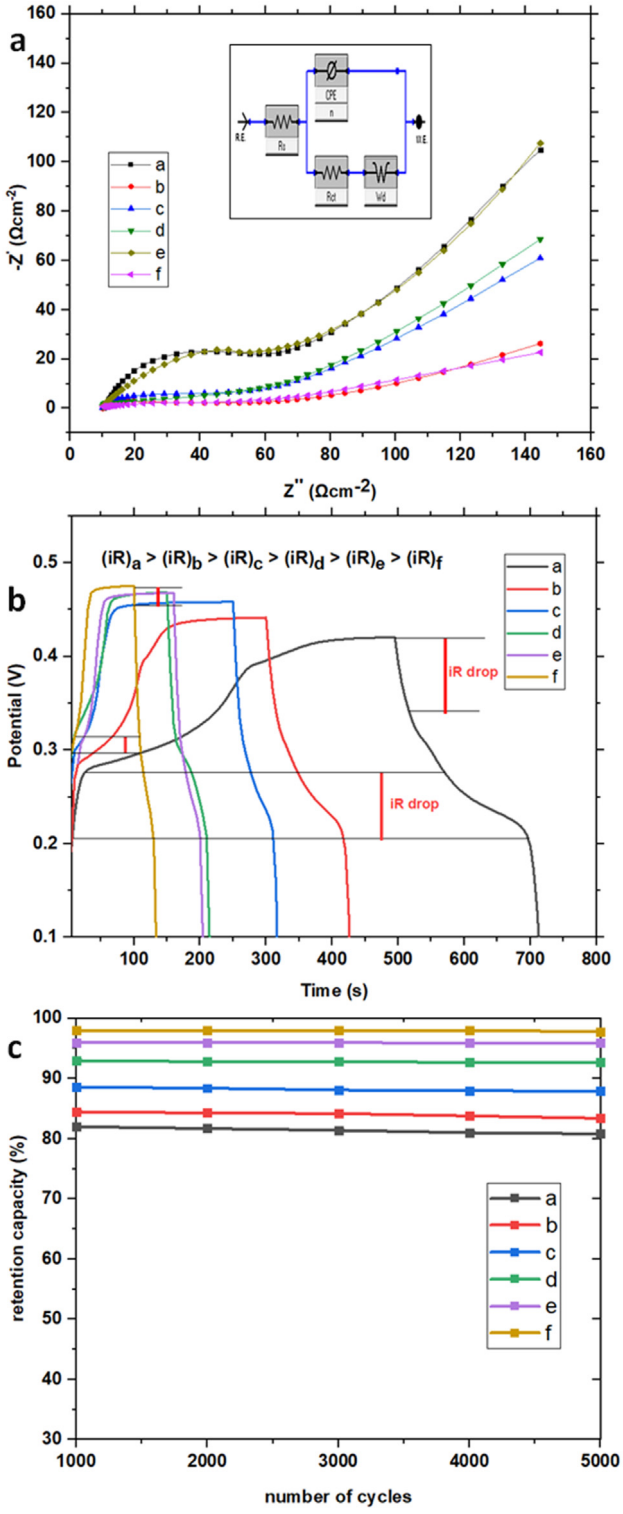

Fig. 7 (a) EIS (b) GCD (c) Retention capacity of the activated forms of (a) starch nanoparticles (b) gelatin nanoparticles (c) starch-gelatin nanohybrids (d) starch-TiO_2 nanohybrids (e) gelatin-TiO_2 nanohybrids (f) starch-gelatin-TiO_2 nanohybrids, at scan rates of 5, 10, 20, 50, 100 and 200 mVs^{-1}.

values of 286, 502, 581, 644, 726 and 808 Fg^{-1}. Whenever the activated starch and gelatin nano-hybrids were combined, there was an increase in the amount of surface oxygen available, hence, higher pseudo-capacitive faradaic charges which contributes to their higher specific capacitance values. This is the first time such a high specific capacitance has been reported for electrochemical tests utilising negative voltages for supercapacitor applications. This confirms that our conductive biopolymer-based nano-architecture can be applied in areas which depend on negative voltages like op-amp circuits, signal control systems, smart switches, and corrosion inhibition.

At scan rates of 200, 100, 50, 20, 10 and 5 mVs^{-1}, the activated starch nanoparticles showed energy density (E_d) values of 12.3, 19.7, 22.8, 36.1, 57.3 and 80.6 $WhKg^{-1}$. The activated gelatin nanoparticles showed E_d values of 12.9, 24.8, 26.1, 43.5, 70.41 and 108.3 $WhKg^{-1}$. The nanohybrids of both the activated starch and gelatin nanoparticles showed E_d values of 19.1, 26.2, 26.8, 59.2, 93.6 and 126.5 $WhKg^{-1}$. After TiO_2 incorporation, activated starch-TiO_2 nanohybrid had E_d values of 30.8, 38.7, 43.2, 71.0, 103.8 and 137.2 $WhKg^{-1}$, activated gelatin-TiO_2 hybrid had E_d values of 36.3, 42.4, 49.0, 78.6, 109.3 and 159.4 $WhKg^{-1}$, while activated starch-gelatin-TiO_2 nanohybrid had E_d values of 52.1, 61.9, 73.6, 92.1, 145.7 and 208.3 $WhKg^{-1}$ (Table 2).

High energy densities in supercapacitors, which are based on conductive polymers, are a result of the presence of permissive polarons and bipolarons which gives room for fast electronic kinetics and diffusion (Ramadoss and Kim, 2014) (Xiong et al., 2016). The power density was 2704, 2791, 2912, 3461, 3813, and 4213 WKg^{-1} for the respective activated forms of starch nanoparticles, gelatin nanoparticles, starch-gelatin nanohybrids, starch-TiO_2 nanohybrid, gelatin-TiO_2 nanohybrid, starch-gelatin-TiO_2 nanohybrid. In Table 2, W is the Warburg impedance, which estimates the diffusional behaviour of the electrodes, CPE is constant phase element, which estimates the capacitance of an unsmooth electrode surface, and n is a CPE index which shows the capacitive capability of the electrode system.

Nyquist plots can be used to investigate the electron transfer kinetics within supercapacitor electrodes (Kim et al., 2016), Fig. 7 presents the Nyquist plots for the biopolymer-based nano-hybrids in 1 M-Na_2SO_4. The EIS showed ohmic resistance values of 0.110, 0.107, 0.104, 0.101, 0.101, 0.087 ohms corresponding to the equivalent series resistances for the nano-hybrids ***a*** to ***f***. The diameter of the semicircles at the moderate frequency region indicates the type of ionic diffusion and level of charge transfer resistance (Xu et al., 2015). Generally, high charge transfer resistances also known as electrochemical system resistance show low capacitances. The charge transfer resistances of starch-TiO_2 nanohybrid, gelatin-TiO_2 nanohybrid, starch-gelatin-TiO_2 nanohybrid were 0.34, 0.31, and 0.29 micro-ohms, which is relatively lower when compared with 0.43, 0.40, 0.39 micro-ohms of starch nanoparticles, gelatin nanoparticles, starch-gelatin nanohybrids without TiO_2 (see Fig. 7).

The electrochemical performances of the nanohybrids were investigated using galvanostatic charge–discharge (GCD). The GCD curves are shown in Fig. 7 (b) at 1 Ag^{-1} current density. Generally, all the GCD curves showed nearly symmetrical patterns indicating a good super-capacitive behaviour (Kumar et al., 2019; Nagamuthu et al., 2013). At 1 Ag^{-1}, the activated starch nanoparticles, gelatin nanoparticles, and starch-gelatin nanohybrid showed iR drop of 0.2, 0.16 and 0.13 ohms. After TiO_2 incorporation, Starch-TiO_2, gelatin-TiO_2 and starch-gelatin-TiO_2 nanohybrids showed a lower iR of 0.13, 0.08,

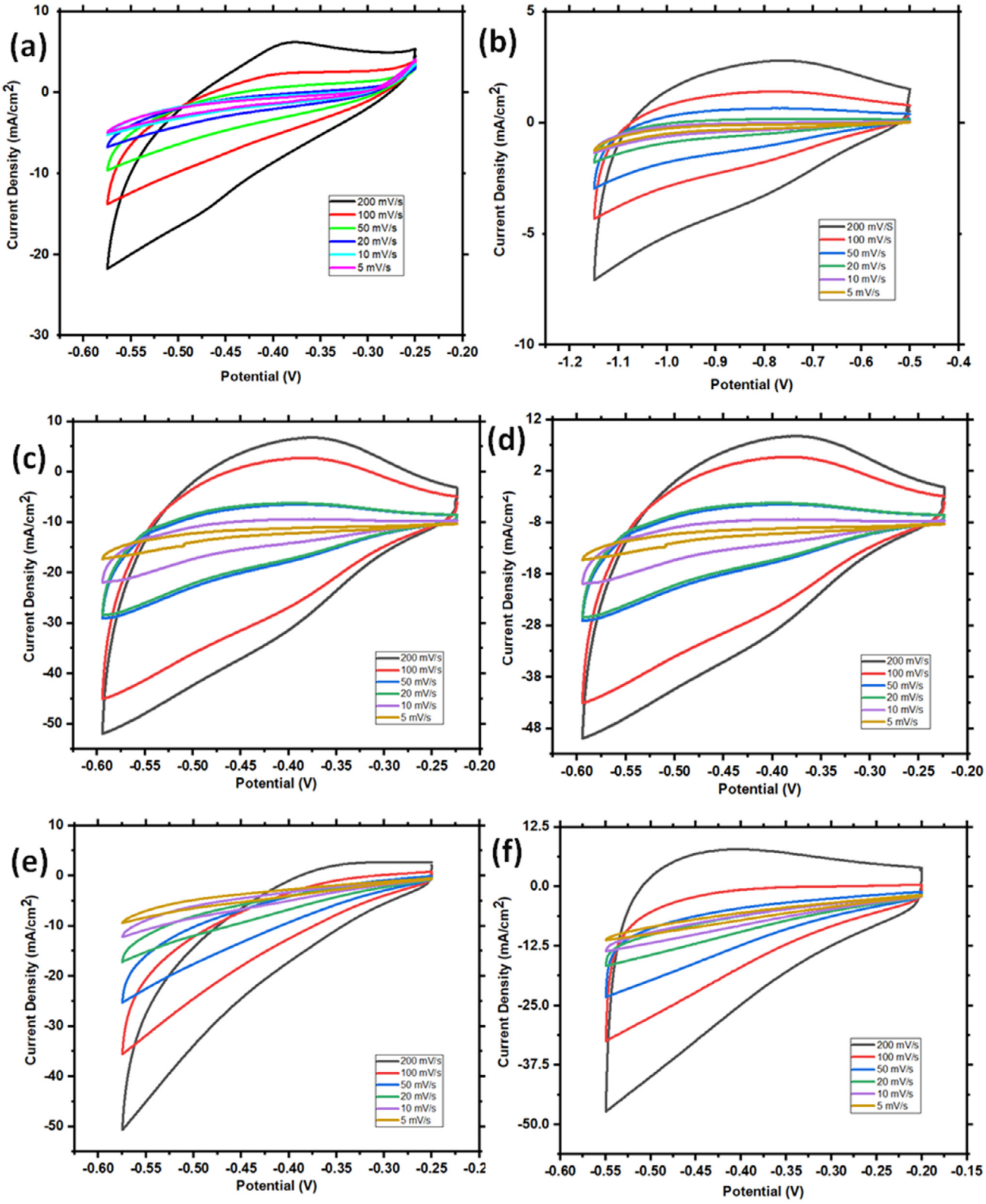

Fig. 8 (Two electrode configuration) CV of the activated forms of (a) starch nanoparticles (b) gelatin nanoparticles (c) starch-gelatin nanohybrids (d) starch-TiO_2 nanohybrids (e) gelatin-TiO_2 nanohybrids (f) starch-gelatin-TiO_2 nanohybrids, at scan rates of 5, 10, 20, 50, 100 and 200 mVs^{-1}.

Table 3 Specific capacitance, energy density and constant phase element (CPE) model parameters for the respective nanohybrids prepared, in two electrode configurations.

Sample	Scan rate (mVs^{-1})					
Activated forms of:	200	100	50	20	10	5
AS-NPs	47	83	106	148	171	194
AG-NPs	70	107	122	156	173	204
ASG-NH	133	170	204	238	260	287
AS-TiO_2 NH	203	355	427	515	531	541
AG-TiO_2 NH	231	356	431	522	540	570
ASG-TiO_2 NH	286	371	442	537	548	617
	Energy density ($WhKg^{-1}$)					
AS-NPs	9.6	12.4	16.0	26.5	34.2	57.9
AG-NPs	10.8	19.2	25.5	38.4	51.8	89.5
ASG-NH	13.8	25.1	31.0	49.7	76.9	105.7
AS-TiO_2 NH	17.1	33.4	42.7	63.6	94.8	122.6
AG-TiO_2 NH	20.1	40.8	44.2	69.1	105.9	138.7
ASG-TiO_2 NH	22.3	53.1	65.0	79.6	116.4	147.4
	R_s	ESR	R_{ct}	W	CPE	n
AS-NPs	0.23	0.152	0.91	2.96	0.13	0.42
AG-NPs	0.23	0.150	0.90	2.92	0.11	0.47
ASG-NH	0.22	0.150	0.88	2.84	0.11	0.52
AS-TiO_2 NH	0.21	0.146	0.68	2.49	0.10	0.57
AG-TiO_2 NH	0.20	0.142	0.65	2.41	0.08	0.60
ASG-TiO_2 NH	0.18	0.115	0.51	2.16	0.07	0.62

0.06 ohms respectively. Also, the potential drop decreases as the ESR decreases for all the nanohybrid electrodes due to rapid diffusion pathways (Sun et al., 2018), which was confirmed from the previously EIS experiments (see Fig. 7(a)). The relatively high polarization resistance might be due to uneven distribution of active materials at higher charging levels, higher viscosity of the electrolyte as the biopolymers are leached into the electrolyte rates (Kim et al., 2016; Zhang et al., 2019). This can be reduced through use of solid electrolytes.

The cycling stabilities of the nanoarchitectures were studied by using 5000 cycles. After 5000 cycles, a capacitance retention of 95.5, 94, 92, 87, 83, 81% was observed for the six respective nanoarchitectures fabricated. The capacitance loss in nanohybrids without TiO_2 incorporation has been demonstrated to arise from the volume swelling and the structure relaxation of the materials caused by the intercalation and dissociation of dopant anions during the long-time charging and discharging processes (Xu et al., 2011, 2015). Although, TiO_2 frameworks helped to stabilize starch-gelatin templates thereby reducing the swelling and shrinking rate of the starch and gelatin, during the charging/discharging period.

3.4. Two electrode configuration electrochemical study

The supercapacitive performance of the novel materials was also studied using two electrode systems to establish the specific capacitance, energy density, power density and retention capacity of the starch-gelatin-TiO_2 nano-hybrids. A symmetric supercapacitor assembly was designed to achieve this study. Overall, the specific capacitances followed similar trends as was observed with the three electrode configurations, and the cyclic voltammetry curves that were quasi rectangular maintained their shape even at higher scan rates. Activated starch nanoparticles had C_{sp} of 47, 83, 106, 148, 171 and 194 Fg^{-1}. The activated gelatin nanoparticles had C_{sp} of 70, 107, 122, 156, 173, and 204 Fg^{-1}. The activated starch-gelatin had C_{sp} of 133, 170, 204, 238, 260, and 287 Fg^{-1}. After TiO_2 incorporation, activated starch-TiO_2 had a C_{sp} of 203, 335, 427, 515, 531 and 541 Fg^{-1}, while the activated gelatin-TiO_2 showed C_{sp} of 231, 356, 431, 522, 540 and 570 Fg^{-1}, and the starch-gelatin-TiO_2 nanohybrids showed C_{sp} of 286, 371, 442, 537, 548 and 617 Fg^{-1}. The data is summarised in Table 3.

Elmouwahidi et al., prepared a series of carbon xerogels doped with different percentages of TiO_2. A high specific capacitance of 137F/g at 0.250 A/g was obtained for 20% TiO_2 incorporation. He further reported a retention capacity of 66–80%. Naeem et al., reported an energy density of 81 Wh/Kg and a specific capacitanc eof 2332F/g for a TiO_2 nano-memberane with controlled thickness fabricated by atomic layer deposition. Our work showed a higher specific capacitance and energy density than most of the similar literatures available on carbons, starch, gelatin and TiO_2 nanomaterials. This is as a result of the activation process carried out to reduce the overall resistance of the biopolymers used. This succesful electrochemical testing on two electrode configurations at negative potential windows has helped to confirm that supercapcitors can now be applied in areas of voltage amplifier circuits which depends on negative voltages for gain stability and decreased output impedance. The effect of positive charges at the oxygen vacancy sites within the starch-gelatin-TiO_2 bionanoarchitectures also contributes to this high electrochemical performance at two electrodes configurational level (Elmouwahidi et al., 2018; Fukuhara et al., 2016; Naeem et al., 2019) (see Fig. 8).

In the two-electrode configuration, at scan rates of 200, 100, 50, 20, 10 and 5 mVs^{-1}, the activated starch nanoparticles

showed energy density (E_d) values of 9.6, 12.4, 16.0, 26.5, 34.2 and 57.9 $WhKg^{-1}$. The activated gelatin nanoparticles showed E_d values of 10.8, 19.2, 25.5, 38.4, 51.8 and 89.5 $WhKg^{-1}$, while activated starch-gelatin-nanohybrid showed E_d values of 13.8, 25.1, 31.0, 49.7, 76.9, and 105.7 $WhKg^{-1}$. After TiO_2 incorporation, activated starch-TiO_2 had E_d values of 17.1, 33.4, 42.7, 63.6, 94.8, and 122.6 $WhKg^{-1}$. The activated gelatin-TiO_2 nanoparticles had E_d values of 20.1, 40.8, 44.2, 69.1, 105.9 and 138.7 $WhKg^{-1}$. The activated starch-gelatin-TiO_2 nanohybrid had E_d values of 22.3, 53.1, 65.0, 79.6, 116.4, and 147.4 $WhKg^{-1}$, as summarised in Table 3. The power density values were 1983, 2554, 2804, 3005, 3527 and 3742 WKg^{-1} for the six respective nanohybrids,.

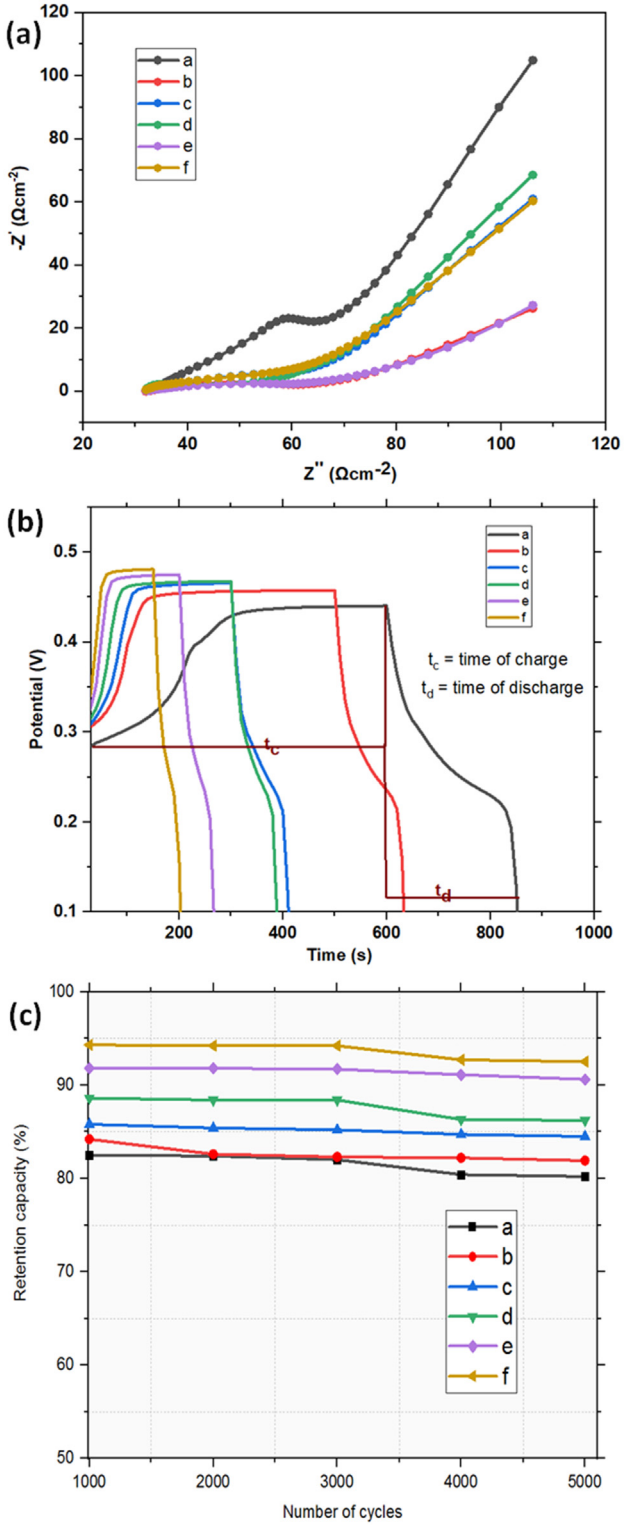

Fig. 9 (a) EIS (b) GCD (c) Retention capacity of the activated forms of (a) starch nanoparticles (b) gelatin nanoparticles (c) starch-gelatin nanohybrids (d) starch-TiO_2 nanohybrids (e) gelatin-TiO_2 nanohybrids (f) starch-gelatin-TiO_2 nanohybrids, at scan rates of 5, 10, 20, 50, 100 and 200 mVs^{-1}.

The EIS (Fig. 9), was carried out to analyse the electrostatic contribution and the resistance elements of the nano-hybrids prepared in the symmetric supercapacitor forms from 0.1 Hz to 1 MHz. The data fitted well into a vertically linear Nyquist plot as produced by the Constant Phase Element model used. Also, from Fig. 9, a rapid increase in the imaginary impedance was seen as compared with the real impedance at the lower frequency regions (Srivastava and Karna, 2015). This capacitive behaviour near the −90° phase angle is a clear confirmation that the starch-gelatin-TiO_2 based supercapacitive nanohybrids are good materials for supercapacitor fabrication. The charge transfer resistance is 0.91, 0.90, 0.88, 0.68, 0.65 and 0.51 ohms; for the six respective nanohybrids.

The GCD plot in Fig. 9 showed similar shapes to those observed with the three electrode configurations, and the charge–discharge times decreased after the incorporation of nano-TiO_2. The increased charge–discharge time after the nano-TiO_2 incorporation is due to the abundance of nano-level tunnels, which are being filled up by the diffusion of polaron and solitons, formed from the diffusion of oxygen radicals within the starch-gelatin-TiO_2 nano-hybrids. The iR drops reduced after the nano-TiO_2 was incorporated, and minor deviations were observed from the GCD linearity, which is expected for supercapacitors because of the rapid anodic oxidation peaks of the oxygen groups in the biopolymers used. The discharge times for all the prepared nanohybrids were shorter than the charge time, typical for energy devices with fast power delivery.

The effect of the rapid anodic oxidation before titanium oxide nanoparticles incorporation was clearly seen in the retention capacity plot. The starch and gelatin nano-architectures had lower retention capacities of 81, 83, and 85% compared with 88, 92, 95% after nano-TiO_2 incorporation. This is because of charge leakages, cracks, surface tears and most importantly rapid anodic oxidation of the available oxygen species, which are slowed down apparently after the oxidation. The retention capacities obtained generally were very good when compared with past works on the use of starch biopolymers for energy storage applications. This high capacity might be due to the use of all our biopolymers in the nano-scale since the quantum-size effect helps to further strengthen the internal interactions thereby improving the overall strength of capacitance retention in the nano-hybrids (Liu et al., 2017).

4. Conclusion

This research shows that new and sustainable supercapacitor electrodes can now be fabricated from starch and gelatin biopolymers to achieve capacity retention as high as 95%. The high charge storage performance in our polymer-based electrodes is as a result of high conductivity from activation,

phase transition of the polymers to more ordered state, and as a result of activation. These biopolymers have good supercapacitive performances at negative potential windows when activated, modified and optimized with pseudo-capacitive nanoparticles. Hence, they can be further applied in signal control systems and smart switches. TiO_2 stabilized starch-gelatin templates, thereby reducing the swelling and shrinking rate of the starch and gelatin during charging and discharging period. The activated starch-gelatin-TiO_2 nanoarchitectures had better structural and electrochemical performance more than other nanoarchitectures designed. The two electrodes configurational electrochemical properties further help to prove the validity of these nano-hybrids for supercapacitor application with higher time constants and lower charge-transfer resistances obtained after activation. Higher energy and power densities obtained in this work make this research a very important one, which can be built upon to further maximize the performance of starch, and gelatin based supercapacitors.

Declaration of Competing Interest

The authors declare that they have no known competing financial interests or personal relationships that could have appeared to influence the work reported in this paper.

Acknowledgements

The National Research Foundation (South Africa) Thuthuka programme, the Centre for Nanomaterials Science Research at the Department of Chemical Sciences (University of Johannesburg), and the URC (University of Johannesburg) funded this work. The authors also thank the Department of Chemical Sciences (University of Johannesburg), and Spectrum (Faculty of Science, University of Johannesburg) for access to research facilities.

References

Capone, I., Hurlbutt, K., Naylor, A.J., Xiao, A.W., Pasta, M., 2019. Effect of the particle-size distribution on the electrochemical performance of a red phosphorus-carbon composite anode for sodium-ion batteries. Energy Fuels 33, 4651–4658.

Chen, H., Shan, Z.H., Woo, M.W., Chen, X.D., 2017. Preparation and characteristic of gelatine/oxidized corn starch and gelatin/corn starch blend microspheres. Int. J. Biol. Macromol. 94, 326–334.

Chong, B.M., Azman, N.H.N., Abdah, M., Aizat, M.A., Sulaiman, Y., 2019. Supercapacitive performance of N-doped graphene/Mn3O4/Fe3O4 as an electrode material. Appl. Sci. 9, 1040.

Ding, C., Qian, X., Yu, G., An, X., 2010. Dopant effect and characterization of polypyrrole-cellulose composites prepared by in situ polymerization process. Cellulose 17, 1067–1077.

Dodoo-Arhin, D., Buabeng, F.P., Mwabora, J.M., Amaniampong, P. N., Agbe, H., Nyankson, E., Obada, D.O., Asiedu, N.Y., 2018. The effect of titanium dioxide synthesis technique and its photocatalytic degradation of organic dye pollutants. Heliyon 4, e00681.

Elmouwahidi, A., Bailón-García, E., Castelo-Quibén, J., Pérez-Cadenas, A.F., Maldonado-Hódar, F.J., Carrasco-Marín, F., 2018. Carbon–TiO 2 composites as high-performance supercapacitor electrodes: synergistic effect between carbon and metal oxide phases. J. Mater. Chem. A 6, 633–644.

Fan, D., Ma, W., Wang, L., Huang, J., Zhao, J., Zhang, H., Chen, W., 2012. Determination of structural changes in microwaved rice starch using Fourier transform infrared and Raman spectroscopy. Starch-Stärke 64, 598–606.

Fan, H., Shen, W., 2015. Gelatin-based microporous carbon nanosheets as high performance supercapacitor electrodes. ACS Sustain. Chem. Eng. 4, 1328–1337.

Finkenstadt, V.L., 2005. Natural polysaccharides as electroactive polymers. Appl. Microbiol. Biotechnol. 67, 735–745.

Fukuhara, M., Kuroda, T., Hasegawa, F., 2016. Amorphous titanium-oxide supercapacitors. Sci. Rep. 6, 35870.

Gopi, C.V.V.M., Vinodh, R., Sambasivam, S., Obaidat, I.M., Kim, H.-J., 2020. Recent progress of advanced energy storage materials for flexible and wearable supercapacitor: from design and development to applications. J. Storage Mater. 27, 101035.

Gu, L., Li, T., Xu, Y., Sun, C., Yang, Z., Zhu, D., Chen, D., 2019. Effects of the particle size of BaTiO3 fillers on fabrication and dielectric properties of BaTiO3/polymer/Al films for capacitor energy-storage application. Materials 12, 439.

Houshyari, A., Heydari, M., Bagheri, M., Nezafati, N., 2018. Preparation of gelatin nanoparticles by a water-in-oil emulsion method for water-soluble model drug encapsulation. Mater. Today:. Proc. 5, 15800–15805.

Hoyos-Leyva, J.D., Alonso-Gomez, L., Rueda-Enciso, J., Yee-Madeira, H., Bello-Perez, L.A., Alvarez-Ramirez, J., 2017. Morphological, physicochemical and functional characteristics of starch from Maranta ruiziana Koern. LWT-Food Sci. Technol. 83, 150–156.

Hu, M., Lei, L., 2007. Effects of particle size on the electrochemical performances of a layered double hydroxide,[Ni 4 Al (OH) 10] NO 3. J. Solid State Electrochem. 11, 847–852.

Ibanez, J.G., Rincón, M.E., Gutierrez-Granados, S., Chahma, M., Jaramillo-Quintero, O.A., Frontana-Uribe, B.A., 2018. Conducting polymers in the fields of energy, environmental remediation, and chemical–chiral sensors. Chem. Rev. 118, 4731–4816.

Jeong, L., Park, W., 2014. Preparation and characterization of gelatin nanofibers containing silver nanoparticles. Int. J. Mol. Sci. 15, 6857–6879.

Kašlík, J., Kolařík, J., Filip, J., Medřík, I., Tomanec, O., Petr, M., Malina, O., Zbořil, R., Tratnyek, P.G., 2018. Nanoarchitecture of advanced core-shell zero-valent iron particles with controlled reactivity for contaminant removal. Chem. Eng. J. 354, 335–345.

Kasturi, P.R., Ramasamy, H., Meyrick, D., Lee, Y.S., Selvan, R.K., 2019. Preparation of starch-based porous carbon electrode and biopolymer electrolyte for all solid-state electric double layer capacitor. J. Colloid Interface Sci. 554, 142–156.

Khan, K., Tareen, A.K., Aslam, M., Mahmood, A., Zhang, Y., Ouyang, Z., Guo, Z., Zhang, H., 2019. Going green with batteries and supercapacitor: two dimensional materials and their nanocomposites based energy storage applications. In: Progress in Solid State Chemistry, p. 100254.

Kim, M., Im, J., Yu, J.-D., Kitae, P., Kwon, O., 2014. Negative voltage generator, decoder, nonvolatile memory device and memory system using negative voltage.

Kim, S.-I., Kim, S.-W., Jung, K., Kim, J.-B., Jang, J.-H., 2016. Ideal nanoporous gold based supercapacitors with theoretical capacitance and high energy/power density. Nano Energy 24, 17–24.

Kumar, R., Ghoshal, G., Goyal, M., 2019. Synthesis and functional properties of gelatin/CA–starch composite film: excellent food packaging material. J. Food Sci. Technol. 56, 1954–1965.

Kumar, R., Singh, B.K., Soam, A., Parida, S., Sahajwalla, V., Bhargava, P., 2020. In situ carbon-supported titanium dioxide (ICS-TiO 2) as an electrode material for high performance supercapacitors. Nanoscale Adv.

Lal, M.S., Lavanya, T., Ramaprabhu, S., 2019. An efficient electrode material for high performance solid-state hybrid supercapacitors based on a Cu/CuO/porous carbon nanofiber/TiO2 hybrid composite. Beilstein J. Nanotechnol. 10, 781–793.

Li, J., Yun, X., Hu, Z., Xi, L., Li, N., Tang, H., Lu, P., Zhu, Y., 2019a. Three-dimensional nitrogen and phosphorus co-doped carbon quantum dots/reduced graphene oxide composite aerogels with a hierarchical porous structure as superior electrode materials for supercapacitors. J. Mater. Chem. A 7, 26311–26325.

Li, W., Zheng, K., Chen, H., Feng, S., Wang, W., Qin, C., 2019b. Influence of nano titanium dioxide and clove oil on chitosan–starch film characteristics. Polymers 11, 1418.
Liu, D., Wu, Q., Chen, H., Chang, P.R., 2009. Transitional properties of starch colloid with particle size reduction from micro-to nanometer. J. Colloid Interface Sci. 339, 117–124.
Liu, Q., Javed, M.S., Zhang, Cuilin, Li, Y., Hu, C., Zhang, Chengshuang, Lai, M., Yang, Q., 2017. Promoting power density by cleaving LiCoO 2 into nano-flake structure for high performance supercapacitor. Nanoscale 9, 5509–5516.
Liu, S., Zeng, J., 2018. Effects of negative voltage on microstructure and corrosion resistance of red mud plasma electrolytic oxidation coatings. Surf. Coat. Technol. 352, 15–25.
Marvizadeh, M.M., Oladzadabbasabadi, N., Nafchi, A.M., Jokar, M., 2017. Preparation and characterization of bionanocomposite film based on tapioca starch/bovine gelatin/nanorod zinc oxide. Int. J. Biol. Macromol. 99, 1–7.
Mendes, J.F., Paschoalin, R.T., Carmona, V.B., Neto, A.R.S., Marques, A.C.P., Marconcini, J.M., Mattoso, L.H.C., Medeiros, E.S., Oliveira, J.E., 2016. Biodegradable polymer blends based on corn starch and thermoplastic chitosan processed by extrusion. Carbohydr. Polym. 137, 452–458.
Naeem, F., Naeem, S., Zhao, Y., Wang, D., Zhang, J., Mei, Y., Huang, G., 2019. TiO 2 nanomembranes fabricated by atomic layer deposition for supercapacitor electrode with enhanced capacitance. Nanoscale Res. Lett. 14, 92.
Nagamuthu, S., Vijayakumar, S., Muralidharan, G., 2013. Biopolymer-assisted synthesis of λ-MnO2 nanoparticles as an electrode material for aqueous symmetric supercapacitor devices. Ind. Eng. Chem. Res. 52, 18262–18268.
Oleyaei, S.A., Zahedi, Y., Ghanbarzadeh, B., Moayedi, A.A., 2016. Modification of physicochemical and thermal properties of starch films by incorporation of TiO2 nanoparticles. Int. J. Biol. Macromol. 89, 256–264.
Oosthuizen, S.J., Swanepoel, J.J., 2018. Development status of the CSIR-Ti process. MS&E 430, 12008.
Pant, B., Park, M., Park, S.-J., 2019. TiO2 NPs assembled into a carbon nanofiber composite electrode by a one-step electrospinning process for supercapacitor applications. Polymers 11, 899.
Railanmaa, A., Kujala, M., Keskinen, J., Kololuoma, T., Lupo, D., 2019. Highly flexible and non-toxic natural polymer gel electrolyte for printed supercapacitors for IoT. Appl. Phys. A 125, 168.
Ramadoss, A., Kim, S.J., 2014. Enhanced supercapacitor performance using hierarchical TiO2 nanorod/Co (OH) 2 nanowall array electrodes. Electrochim. Acta 136, 105–111.
Reddy, K.M., Sunkara, V.M., Reddy, A.R., 2001. Synthesis of TIO2 Nano Powder by the Sol Gel Method and its use as a Photocatalyst.
Romero, I.S., Schurr, M.L., Lally, J.V., Kotlik, M.Z., Murphy, A.R., 2013. Enhancing the interface in silk–polypyrrole composites through chemical modification of silk fibroin. ACS Appl. Mater. Interfaces 5, 553–564.
Rozendaal, A., Le Roux, S.G., du Plessis, A., Philander, C., 2018. Grade and product quality control by microCT scanning of the world class Namakwa Sands Ti-Zr placer deposit West Coast, South Africa: an orientation study. Miner. Eng. 116, 152–162.
Selvaraj, T., Perumal, V., Khor, S.F., Anthony, L.S., Gopinath, S.C. B., Mohamed, N.M., 2020. The Recent Development of Polysaccharides Biomaterials and Their Performance for Supercapacitor Applications. Materials Research Bulletin, p. 110839.
Sharma, L., Sharma, H.K., Saini, C.S., 2018. Edible films developed from carboxylic acid cross-linked sesame protein isolate: barrier, mechanical, thermal, crystalline and morphological properties. J. Food Sci. Technol. 55, 532–539.
Soliman, E.A., Furuta, M., 2014. Influence of phase behavior and miscibility on mechanical, thermal and micro-structure of soluble starch-gelatin thermoplastic biodegradable blend films. Food Nutrit. Sci. 5, 1040.
Sondari, D., Aspiyanto, Amanda, A.S., Triwulandari, E., Ghozali, M., Septiyanti, M., Iltizam, I., 2018. Characterization edible coating made from native and modification cassava starch. In: AIP Conference Proceedings. AIP Publishing, p. 30013.
Srivastava, A.K., Karna, S., 2015. Studies on High Energy Density Reactions for Development of Nanostructured Hybrid Supercapacitors. Mumbai Univ, India.
Subara, D., Jaswir, I., Alkhatib, M.F.R., Noorbatcha, I.A., 2018. Synthesis of fish gelatin nanoparticles and their application for the drug delivery based on response surface methodology. Adv. Nat. Sci.: Nanosci. Nanotechnol. 9, 45014.
Sun, S., Sun, Y., Wen, J., Zhang, B., Liao, X., Yin, G., Huang, Z., Pu, X., 2018. MoO 3− x-deposited TiO 2 nanotubes for stable and high-capacitance supercapacitor electrodes. RSC Adv. 8, 21823–21828.
Tay, S.H., Pang, S.C., Chin, S.F., 2012. A facile approach for controlled synthesis of hydrophilic starch-based nanoparticles from native sago starch. Starch-Stärke 64, 984–990.
Wang, C.M., Wen, C.Y., Che, Y.C., Chang, J.-Y., Ho, C.H., Kao, K.-S., Shih, W.C., Chiu, C.-M., Shen, Y.A., 2015. The influence of specific surface area on the capacitance of the carbon electrodes supercapacitor. In: The Proceedings of the Second International Conference on Industrial Application Engineering, pp. 439–442.
Wang, L.W., Wang, X.H., Cui, Z.Y., Liu, Z.Y., Du, C.W., Li, X.G., 2014. Effect of alternating voltage on corrosion of X80 and X100 steels in a chloride containing solution–investigated by AC voltammetry technique. Corros. Sci. 86, 213–222.
Warren, F.J., Gidley, M.J., Flanagan, B.M., 2016. Infrared spectroscopy as a tool to characterise starch ordered structure—a joint FTIR–ATR, NMR, XRD and DSC study. Carbohydr. Polym. 139, 35–42. https://doi.org/10.1016/j.carbpol.2015.11.066.
Wu, S., Yu, B., Wu, Z., Fang, S., Shi, B., Yang, J., 2018. Effect of particle size distribution on the electrochemical performance of micro-sized silicon-based negative materials. RSC Adv. 8, 8544–8551.
Xia, X., Li, G., Liao, F., Zhang, F., Zheng, J., Kan, J., 2015. Granular structure and physicochemical properties of starches from amaranth grain. Int. J. Food Prop. 18, 1029–1037.
Xiong, Q., Zheng, C., Chi, H., Zhang, J., Ji, Z., 2016. Reconstruction of TiO2/MnO2-C nanotube/nanoflake core/shell arrays as high-performance supercapacitor electrodes. Nanotechnology 28, 55405.
Xu, C., Sun, J., Gao, L., 2011. Synthesis of novel hierarchical graphene/polypyrrole nanosheet composites and their superior electrochemical performance. J. Mater. Chem. 21, 11253–11258.
Xu, H., Huang, W., Chen, Y., Liu, Z., Shen, X., Zhang, J., Zhu, X., 2019. Fabrication of TiO2 nanowire array on Ti-4Al-0.005 B alloy applied to supercapacitor electrodes. Chem. Phys. Lett. 732, 136656.
Xu, J., Wang, D., Yuan, Y., Wei, W., Duan, L., Wang, L., Bao, H., Xu, W., 2015. Polypyrrole/reduced graphene oxide coated fabric electrodes for supercapacitor application. Org. Electron. 24, 153–159.
Yan, Y., Wang, T., Li, X., Pang, H., Xue, H., 2017. Noble metal-based materials in high-performance supercapacitors. Inorg. Chem. Front. 4, 33–51.
Yang, J., Shen, D., Zhou, L., Li, W., Li, X., Yao, C., Wang, R., El-Toni, A.M., Zhang, F., Zhao, D., 2013. Spatially confined fabrication of core–shell gold nanocages@ mesoporous silica for near-infrared controlled photothermal drug release. Chem. Mater. 25, 3030–3037.
Zhang, Z., Zhang, D., Lin, H., Chen, Y., 2019. Flexible fiber-shaped supercapacitors with high energy density based on self-twisted graphene fibers. J. Power Sources 433, 226711.
Zhou, M., Lyu, Y., Liu, Y., Guo, B., 2019. Porous scaffold of TiO2 for dendrite-free lithium metal anode. J. Alloys Compd. 791, 364–370.